Localized Electroconvection at Ion-Exchange Membranes with Heterogeneous Surface Charge

Felix Stockmeier
DWI - Leibniz Institute for Interactive Materials https://orcid.org/0000-0002-4725-6607
Daniel Felder
DWI - Leibniz Institute for Interactive Materials https://orcid.org/0000-0003-0065-7144
Steffen Eser
DWI - Leibniz Institute for Interactive Materials
Malte Habermann
DWI - Leibniz Institute for Interactive Materials
Petar Peric
DWI - Leibniz Institute for Interactive Materials
Stephan Musholt
DWI - Leibniz Institute for Interactive Materials
Katharina Albert
DWI - Leibniz Institute for Interactive Materials
John Linkhorst
RWTH Aachen University
Matthias Wessling (manuscripts.cvt@avt.rwth-aachen.de)
RWTH Aachen University https://orcid.org/0000-0002-7874-5315

Article

Keywords: Electrodialysis, Electroconvection, Heterogeneity, PTV, DNS

Posted Date: November 23rd, 2021

DOI: https://doi.org/10.21203/rs.3.rs-1093972/v1

Localized Electroconvection at Ion-Exchange Membranes with Heterogeneous Surface Charge

Felix Stockmeier[1,2], Daniel Felder[1,2], Steffen Eser[1,2], Malte Habermann[2], Petar Perić[2], Stephan Musholt[2], Katharina Albert[2], John Linkhorst[1], and Matthias Wessling*[1,2]

[1]RWTH Aachen University, Chemical Process Engineering, Forckenbeckstraße 51, 52074 Aachen, Germany

[2]DWI - Leibniz Institute for Interactive Materials, Forckenbeckstraße 50, 52074 Aachen, Germany

November 17, 2021

Keywords

Electrodialysis, Electroconvection, Heterogeneity, PTV, DNS

*corresponding author
manuscripts.cvt@avt.rwth-aachen.de

Abstract

Operating electrochemical membrane processes beyond the limiting current density bears the potential to decrease the investment cost of desalination plants significantly. However, while there are strategies for successfully reducing energy demand by shortening the plateau region, their influence on the formation of electroconvection is still unknown.

This study demonstrates control over the electroconvective vortices' rotational direction and position using a surface patterning method. We compare the development of electroconvection at two membranes modified with patterns of different surface charges. We analyze the electroconvective vortex field's build-up, the vortices' rotational direction, and structural stability in the steady-state. Finally, we showcase the control possibilities by enforcing a specific structure along an asymmetric letter pattern. Such tailor-made patterns have the potential to diminish the plateau region's energy loss completely. Furthermore, the scale-up of these membranes to industrial processes will allow the economic operation in the overlimiting regime, significantly increasing their space-time yield.

Introduction

The operation range of electrically driven membrane processes like electrodialysis (ED), capacitive deionization (CDI), and flow-capacitive deionization (FCDI) is limited by the fluid-sided resistance evolving during operation at high driving force [1]. In these processes, ions are transported through charge-selective membranes by an electric field. The ion flow, measured as a current density, increases linearly with increasing driving force in terms of an electric potential between two electrodes. However, the current increase is disrupted by a diffusion-limited plateau region (see Fig. 1 **a)**) [1]. Today, it is known that a significant share of the current increase is due to a hydrodynamic instability called electroconvection (EC). EC overcomes the

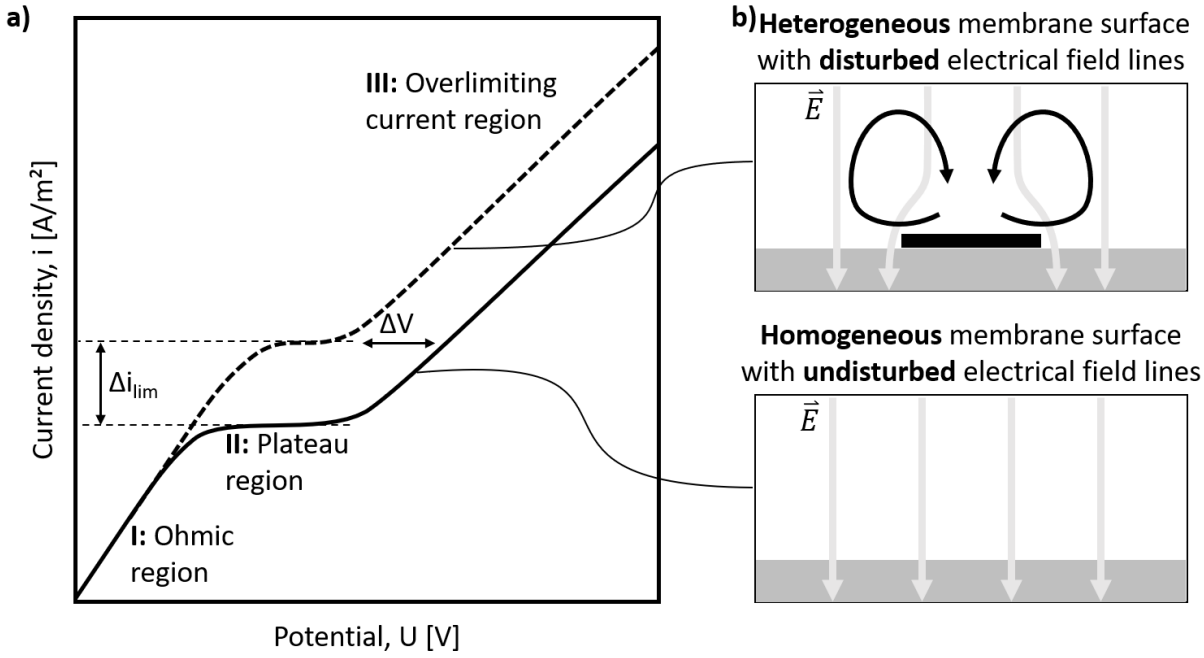

Figure 1: **Current density over potential graph for a homogeneous and heterogeneous membrane and difference in electric field lines. a)** Sketch of the current density over potential graph for an electrically driven membrane process with a homogeneous (solid line) or heterogeneous (dashed line) membrane. For both cases, three distinct regimes appear with a difference in the limiting current density i_{lim}. **b)** Electric field lines at a homogeneous and heterogeneous membrane surface.

limiting current density due to the formation of convective 3D vortices, recently quantified by Stockmeier et al. [2], which mix the depleted layer close to the membrane. In fact, EC balances with unwanted water splitting and a maximum contribution of EC to the overlimiting current density is desired [3].

The possibility to evoke and intensify EC also at low driving forces has been the focus of multiple studies [4–13]. In general, the limiting current density and the length of the plateau region have been found to depend on the ion concentration, distance between the bulk electrolyte and membrane (i.e., the laminar boundary layer), and membrane characteristics like surface heterogeneity [1]. A heterogeneous membrane surface causes a disturbance of the electrical field lines close to the membrane, which, in turn, triggers EC, see Fig. 1 **b)**. As a result, the plateau is shortened. The results of Roghmans et al. [11] suggest that EC even emerges in the ohmic region at their pattern structure, increasing the limiting current density.

Modifying membranes as a means to control surface heterogeneity has gained increasing interest in the literature. Various studies focused on heterogeneity in surface geometry, conductivity, hydrophobicity, and zeta potential. It has been shown that these four parameters, in particular, have a significant influence on the formation of electroconvection and the rotational direction of the vortices. [11, 14–23].

To elucidate the effect of a 2D geometrically heterogeneous surface, Valenca et al. recorded the velocity and orientation of EC vortices at a patterned cation-exchange membrane using 2D particle image velocimetry [8]. The membrane was cast onto a linear gird, creating a surface topology with valleys and hills. Their recordings revealed the formation of pairs of counter-rotating vortices at the ridges of the pattern. The rotation of these vortices was directed towards the patterns' valleys, which resulted in the transport of ion-rich bulk solution towards the valleys. Overall, the 2D geometrically heterogeneous surface decreased the system's resistance

of about 50%.

A similar observation was made by Davidson et al. in 2D DNSs at a membrane patterned with non-conductive sections [7]. Although these patterns did not alter the membrane's geometry, vortices formed at the pattern's edges and rotated towards the patches' centers. This rotational direction results in the transport of ion-rich bulk solution towards the non-conductive patches. Even though the existence of patches increased the overall ion transport and strength of EC, one can imagine that membranes with similar EC-enhancing properties but either ion-conductive patches or a vortex field that transport ion-rich solution towards the free membrane surface will result in even more increased ion transport. They found that the optimal pattern length for a stable vortex structure and highest current density correlated with the diffusion boundary layer's height.

Kim et al. ranked the current increase of different, spacer-like structures on top of the membrane surface under forced flow [12]. They found that segmentation of the boundary layer and, therefore, creating intentional dead zones is beneficial for the build-up of EC. Square patterns, forming large dead zones, resulted in the highest vortex intensity in the overlimiting regime.

Recently, we presented a method to simultaneously engineer the surface geometry, conductivity, and charge of membrane surfaces in a controlled manner [11]. An ink-jet printing technique was used to apply a pattern of circular patches of polymer microgels with varying zeta potential. Such modified membranes were found to double the limiting current density with a 40% reduced plateau length and only slightly increased membrane resistance. The hypothesis behind this successful modification was a combination of an early start of EC even at limiting current densities, the ion conductivity of the pattern, an altered rotational direction due to the direction of the surface charge gradient, and the formation of a 3D vortex pattern compared to the 2D structures of Valenca et al. and Davidson et al. Davidson et al. [7], de Valenca et al. [8].

The examples mentioned above show the vast potential that engineered ion-exchange membranes with tailored surface properties possess to increase the efficiency of electrically driven membrane processes. However, the physics behind the current density increase, especially of Roghmans et al.'s multi-influential microgel patterns, are still unclear. Therefore, the EC vortex field structure at such patterns needs to be analyzed, isolating important properties for future membrane modifications.

In this paper, we evaluate the effect of patterning a cation-exchange membrane surface, with the technique described by Roghmans et al., on the 3D hydrodynamics of EC using micro particle tracking velocimetry (µPTV) [2, 11]. Our numerical and experimental investigation aims at revealing the effect of patterning the membrane surface on the electroconvective vortex field. First, we analyze the orientation of coherent vortex structures and their rotational direction in 2D direct numerical simulations (DNSs) and confirm these results by recording the 3D velocity field during its build-up close to a modified membrane with µPTV. We then affirm that a change in the vortex structure compared to an unmodified membrane also persists in the steady-state of our experiments. At last, we conclude the potential of the findings by exploring the possibility of fully controlling and shaping EC's vortex field with our modification method.

Results and discussion

Vortex orientation and rotational direction at heterogeneous surface charge - simulation

We performed 2D simulations in a rectangular domain with an aspect ratio of 6 described in detail in the Methods section. The simulations assume a potential difference between the top reservoir and the ideal bottom cation-exchange membrane.

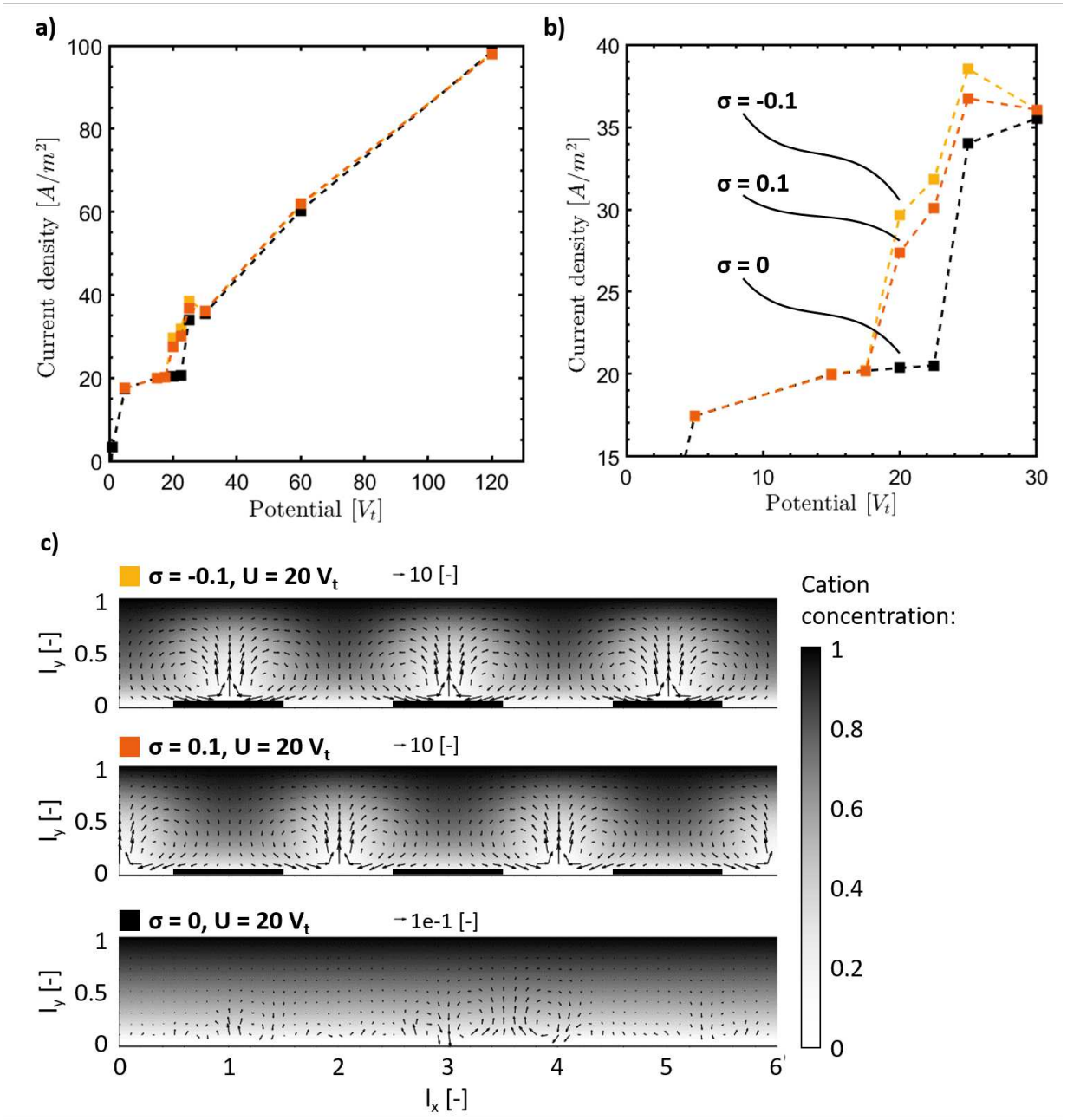

Figure 2: **Simulation results for current densities, vortex structure, and rotational direction.** **a)** shows the current density over potential plot for an untreated membrane, two patched membrane one with positive and one with negative zeta potential. **b)** shows an enlarged graph of the plateau region seen in **a)**. **c)** displays the corresponding cation concentration field as gray-scale background and the velocity field as an arrow plot for simulations at 20 V_t (thermal volts).

Fig. 2 **a)** displays the steady-state current densities over the potential for simulations with patches of 10 % reduced or increased charge ($\sigma = -0.1$ and $\sigma = 0.1$) and the case with homogeneous surface charge ($\sigma = 0$). In all three cases, the plateau starts at a potential of 5 V_t with a limiting current density of 20 A m^{-1}. For the case with homogeneous surface charge ($\sigma = 0$), the plateau region extends to 22.5 V_t, transitioning in the overlimiting current density at 25 V_t with a linearly increasing current density thereafter.

The simulations with patches both show a shortened plateau region that ends at 15 V_t. The overlimiting current region starts at 17.5 V_t. However, the graphs do not steadily increase. Instead, both exhibit a local minimum at 30 V_t again overlapping with the patch-less case graph showing a similar increase from thereon. This behavior indicates that the patches' influence dwindles with increasing potential. The experimental study of Roghmans et al. [11] showed a more pronounced effect even in the overlimiting region, indicating that our simulation does not consider all relevant effects. Still, these results provide valuable insights into the physics at play.

Fig. 2 **b)** shows a zoom on the transition through all three regions. The zoom reveals that the current densities of the simulation with negative patch charge reach up to 8.4% higher values at the beginning of the overlimiting current region compared to the positive charge case. This difference possibly results from the 15.6% higher root mean square velocity in the first case, which might, in turn, originate from the membrane's higher net charge as EC depends on the concentration gradient close to the membraneμ [1].

The images in Fig. 2 **c)** show the steady-state of simulations at 20 V_t for all three cases. The gray-scale background indicates the cation concentration, and the overlaid arrows show the velocity field.

At the membrane with homogeneous surface charge ($\sigma = 0$), the cation concentration gradient

between bulk and membrane stays constant over the channel's width. As a result, emerging velocities are small with little vorticity and maximum velocities in the order of $1 \cdot 10^{-5}$.

For patched membranes, convection cells of low concentration emerge as light gray areas that span from the membrane to close to the bulk phase. Inside the convection cells, velocities are larger than two orders of magnitude than for a homogeneous membrane and are directed towards the bulk. Between the cells, the velocities are directed towards the membrane. This way, vortex pairs form inside the cells. In both simulations ($\sigma = -0.1$ and $\sigma = 0.1$) the convection cells locate above the regions with more negative surface charge.

These results indicate that the patches lead to early and strong EC development even at potentials where the homogeneous membrane shows limiting current densities. In addition to the early EC occurrence, the regular patch pattern leads to the EC vortex field's orientation alongside that pattern. In combination with the relative surface charge change, this orientation dictates the positions of the low concentration cells and, therefore, the rotational direction of the EC vortices above the patches. The resulting current densities predict that the rotation of vortices toward the bare membrane between patches in the negative charge case is favorable. To validate the findings of the 2D simulations, namely the change in rotational direction and localization of vortex field features, 3D experiments were conducted with membranes modified with patches of defined surface charge contrast to the base material.

Vortex orientation and rotational direction at heterogeneous surface charge - experiment

Fig. 3 **a)** shows a top view on the 3D velocity field measured at $4 \cdot i_{\mathrm{lim}}$ between the anode and an untreated membrane. The velocities are plotted in a symmetric red, white, and blue spectrum on iso-surfaces of coherent vortex structures.

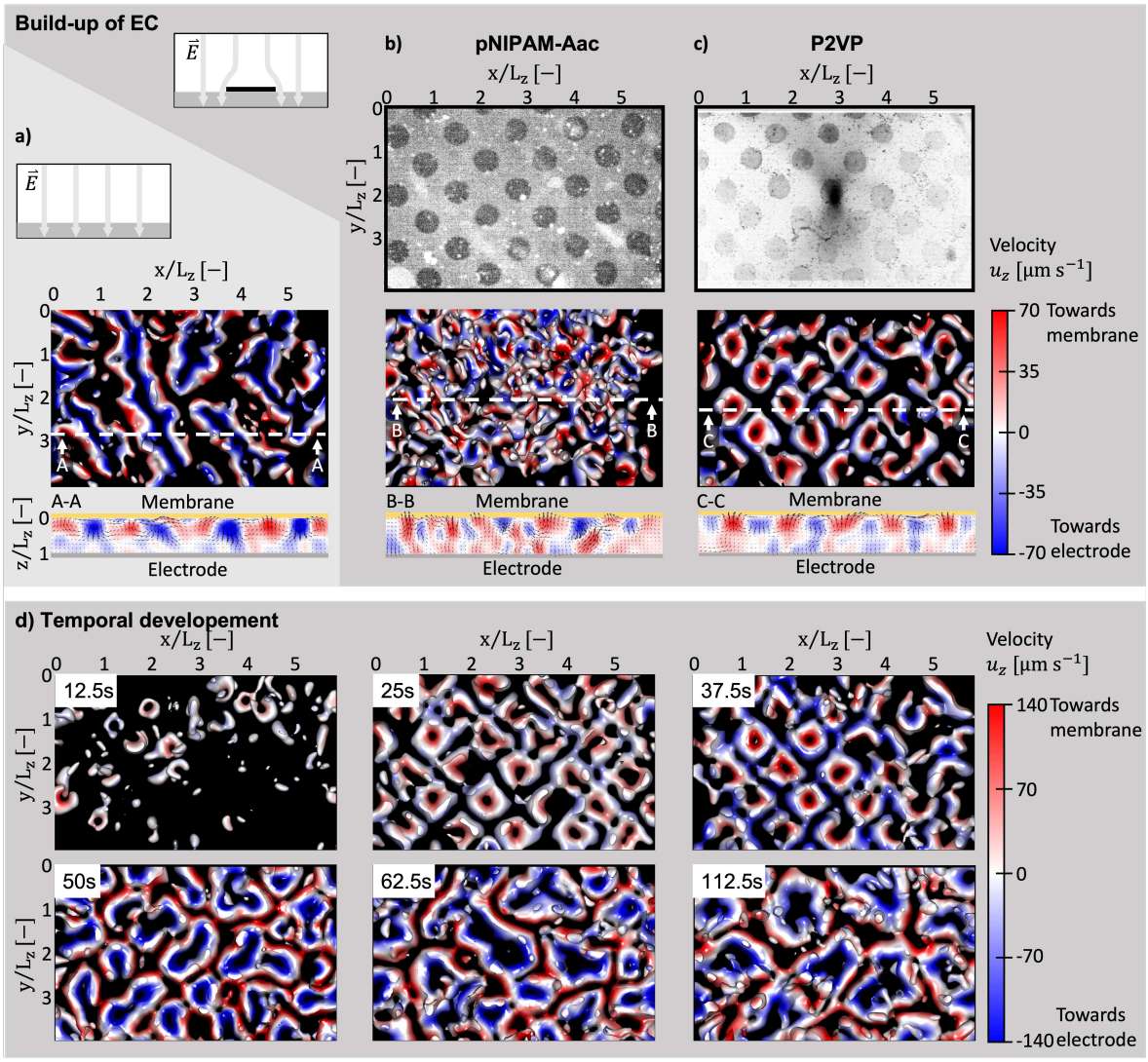

Figure 3: **Vortex structure and rotational direction during electroconvection. a)** Top view on the steady-state vortex structure and cross-section of the velocity field developing at a bare membrane. **b)** & **c)** Patch patterns, vortex structures, and velocity fields for membranes modified with pNIPAM-co-Aac an P2VP microgels, respectively. **d)** Temporal development of the top view on the vortex structure of the experiment shown in **c)** between 12.5 s to 112.5 s. The velocity is colored in magnitude and direction according to the scale bar from blue to red.

The experiment shows a typical, stable vortex roll pattern for relatively small overlimiting current densities visible as linearly stretched coherent vortex structures [2, 24, 25]. These rolls occur as counter-rotating pairs visible as tube-like coherent structures. At spots where multiple roll pairs would collide, the parallel rolls of a pair connect to form a half-circle. The velocity between clearly visible vortex roll pairs is directed towards the electrode indicated by the blue coloring.

The top picture of Fig. 3 **b)** displays the PNIPAM-co-Aac microgel pattern structure with a patch diameter of 400 µm. Despite the patch pattern, no regular structure is visible in the vortex field. However, the structure also differs from the case of an untreated membrane. Instead of vortex rolls, single ring-shaped vortices can be found with velocities in their centers directed towards the membrane.

The P2VP microgel patch pattern in Fig. 3 **c)** is similar to the pattern produced with PNIPAM-co-Aac microgels. Nevertheless, the vortex structure differs to a large degree forming a regular pattern of vortex rings. The vortex ring positions match the patch pattern structure in position and size. Furthermore, this experiment proves validates the simulations in Fig. 2 with the velocities in the centers of rings being directed towards the patches.

The observed transition in Fig. 3 from a regular vortex roll pattern **a)** to an unorganized vortex field **b)**, and an ordered structure **c)** with the introduction of increasing surface charge differences between membrane and pattern shows that a minimum charge difference is necessary to trigger ordered pattern formation. This dependence is supported by additional simulations presented in the supplementary material S2. The zeta potential difference between the Nafion membrane and the PNIPAM-co-Aac patches is not large enough to enforce vortex orientation. However, the introduced heterogeneity is still sufficient to disturb the usual regular vortex

roll pattern seen at an untreated membrane. The P2VP microgel pattern introduces a strong zeta potential contrast towards Nafion, which enforces vortex orientation as predicted by the simulations. The results show a clear and stable vortex formation along the pattern perimeters.

A change in the steady-state is achieved

Fig. 3 **d)** shows a series of snapshots over time of the build-up of EC towards a steady-state for a P2VP microgel treated membrane. The first time step (12.5 s) shows only a small amount of coherent structures without particular order. At 25 s, an ordered structure of vortex rings is clearly visible, as already described in the previous section (see Fig. 3 **c)**). The velocity in the centers of vortex rings is directed towards the patches on the membrane. The structure is preserved at 37.5 s, but the overall velocities are increased. The next snapshot (50 s) shows a different vortex field. The regular structure vanished, showing vortex rings or ellipses of different shapes instead. Additionally, the rotational direction in the vortex ring centers changes towards the electrode, similar to the direction of EC vortex rolls at an untreated Nafion membrane at higher current densities [2]. Later, the chaotic vortex rings approximately double in diameter between 50 s and 62.5 s, which stays constant in the steady-state at 112.5 s. The changed rotational direction is dominant throughout the steady-state. Compared to the case of an untreated Nafion membrane in Fig. 3 **a)**, no vortex roll pattern forms.

The loss of orientation occurs for two reasons. First, the current density of $4 \cdot i_{\mathrm{lim}}$ might already be too large to sustain the orientation. The simulations in supplementary materials S2 show that the electrokinetic forces dominate the patches' influence at current densities increasing beyond 30 V_t. Second, the results of Valenca et al. and Davidson et al. suggest that the optimal 2D pattern size is equal to the boundary layer height [7, 8]. In our experiment, this would be equal to the membrane to electrode distance of 800 µm. However, we chose this

diameter to investigate the influence of a smaller patch diameter on the steady-state vortex field. As a result, the vortex ring diameter doubles from 25 s to 112.5 s, spanning over multiple patches. Interestingly, the presence of the pattern still hinders the formation of the vortex roll structure that would form at an untreated membrane at this current density.

Surface modification offers full control over vortex structure

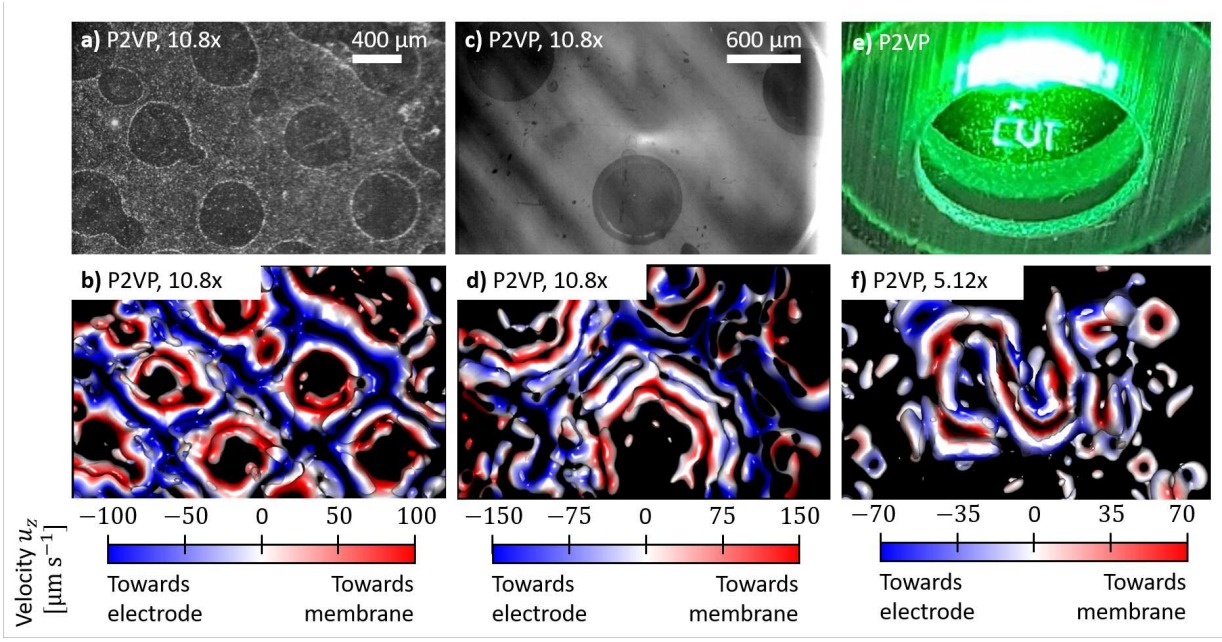

Figure 4: **Complex P2VP microgel pattern proof full control over vortex field. a)** & **c)** P2VP microgel patch pattern with 400 µm and 600 µm diameter show a clear orientation at a magnification of 10.08 ×. **b)** & **d)** Top view of the resulting vortex structures. **e)** Image of the membrane modified with the CVT-logo structure inside the module illuminated by green light. **f)** Top view of the coherent vortex structure after 1.6 s of the experiment at a magnification of 5.12 ×. The velocity is colored in magnitude and direction according to the scale bar from blue to red.

We conducted further experiments at 10.08 × magnification with smaller tracer particles with a diameter of 0.86 µm to better compare the vortex ring and patch positions.

Fig. 4 **a)** and **c)** show two Nafion membranes patterned with P2VP microgels with a 400 µm

diameter and a 600 µm diameter, respectively.

The vortex field reconstruction of the experiments at both membranes is shown in Fig. 4 **b)** and **d)**. In both images, coherent vortex rings emerge that resemble the patterns. Interestingly, the vortices also resemble the slight imperfections in the pattern for the 400 µm case. The rotation of the vortex rings is directed towards the patches as in the experiments at lower magnification with larger particles, see Fig. 3.

The results show that the patches enforce their structure on EC's build-up in its development regardless of shape and size. Furthermore, even slight imperfections in the patches' geometry are reproduced in the vortex structure, demonstrating that complete geometric control of the EC vortex field can be achieved using this membrane modification method. Therefore, we printed our chairs' 'CVT'-lettering to achieve a structure with varying line distances and direction changes. The pattern was produced by printing lines of overlapping circular patches (see Fig. 4 **e)**).

Fig. 4 **f)** shows a snapshot of the vortex structure during the build-up of EC. The vortex field's shape clearly follows the printed structure. The velocity's color map reveals that a pair of vortices builds at the structures with velocity towards the structure in between. This rotational direction was also observed in the previous experiments.

These results prove that the P2VP microgel pattern enforces the build-up of vortex pairs at the structure, completely resembling its shape. The emergence of strong EC vortices only at the structure also shows that a P2VP pattern structure leads to a faster EC build-up. It also gives additional proof that vortices move towards P2VP-coated surfaces.

Conclusions

Our results show that the membrane modification technique offers complete control over the vortex structure of electroconvection.

Patches of P2VP microgels that introduce a large zeta potential contrast to the membrane lead to the structuring of the vortex field. While the patch geometry has an optimum range in current density to structure the vortices, the orientation is lost beyond this range. This behavior allows not only a geometric control of the vortices but also a control of the onset of fully-developed EC at a certain operating point in an electrochemical process. Even with PNIPAM-co-Aac microgel patches, the usual vortex roll pattern observed at homogeneous Nafion membranes is suppressed, although the zeta potential difference contrast is significantly lower. We attribute the effects seen in the experiments of Roghmans et al. [11] in part to this change in the vortex structure. Therefore, future micro- and macroscopic studies should focus on the effect of tailored 3D vortex structures on the limiting current density and plateau length.

Our simulations additionally show that the vortices orientate towards the surface with the higher zeta potential. In accordance, our experiment with P2VP microgel patterns shows localization of vortex rings with a vortex rotational direction towards the patches' centers. Control over the rotational direction of the EC vortex rings was previously hypothesized to be a key to an optimized membrane modification [11]. The experiments presented in this study demonstrate that the geometry and the zeta potential allow for control of the rotational direction of the vortex rings.

The possibility of controlling both the shape and rotational direction of the electroconvective vortex field motivates the development of more complex, transport enhancing modifications of ion-exchange membranes. With the increasing influence of EC, the share of water splitting to the ion transport will also decrease. Additionally, the modification method is easily upscalable to cover larger membrane areas. Further progress will enable efficient use of the overlimiting

current region in industrial-scale processes leading to decreased material and investment costs.

Model problem

We use the open-source, OpenFOAM-based, finite-volume solver rheoTool by Pimenta and Alves to simulate the electroconvective flow driven by an electric field of a symmetric binary electrolyte between an ideal cation-exchange membrane and a reservoir, see Fig. 5 **a)** [26]. The solver couples transport of charged species described by the Poisson-Nernst-Planck equations with the Navier-Stokes equations for fluid flow by viscous drag. In this investigation, we extend rheoTool's 'Charge transport across an ion-selective membrane' case, which is based on the work of Druzgalski et al. [27].

Fig. 5 **a)** shows the 2D rectangular domain, which has an aspect ratio of 6 lengths per height with periodic boundary conditions at each end. The ion transport is driven by the external applied potential difference ΔV between reservoir and membrane. The reservoir boundary condition is implemented as an electro-neutral electrolyte with fixed concentrations. The boundary condition for the ideal cation-exchange membrane has a fixed cation concentration and is impermeable for anions. We add a pattern of patches that introduce additional charge through the location-dependent background charge σ to the membrane surface. The patches are fully ion-permeable, and the complete flow equations are solved inside of them. The length of the patches, as well as their distance to each other, is chosen equal to the domain height, which was shown to evoke an optimal vortex structure when using non-permeable patches [7]. We implement the patches with an aspect ratio of 100, similar to our previous study [11].

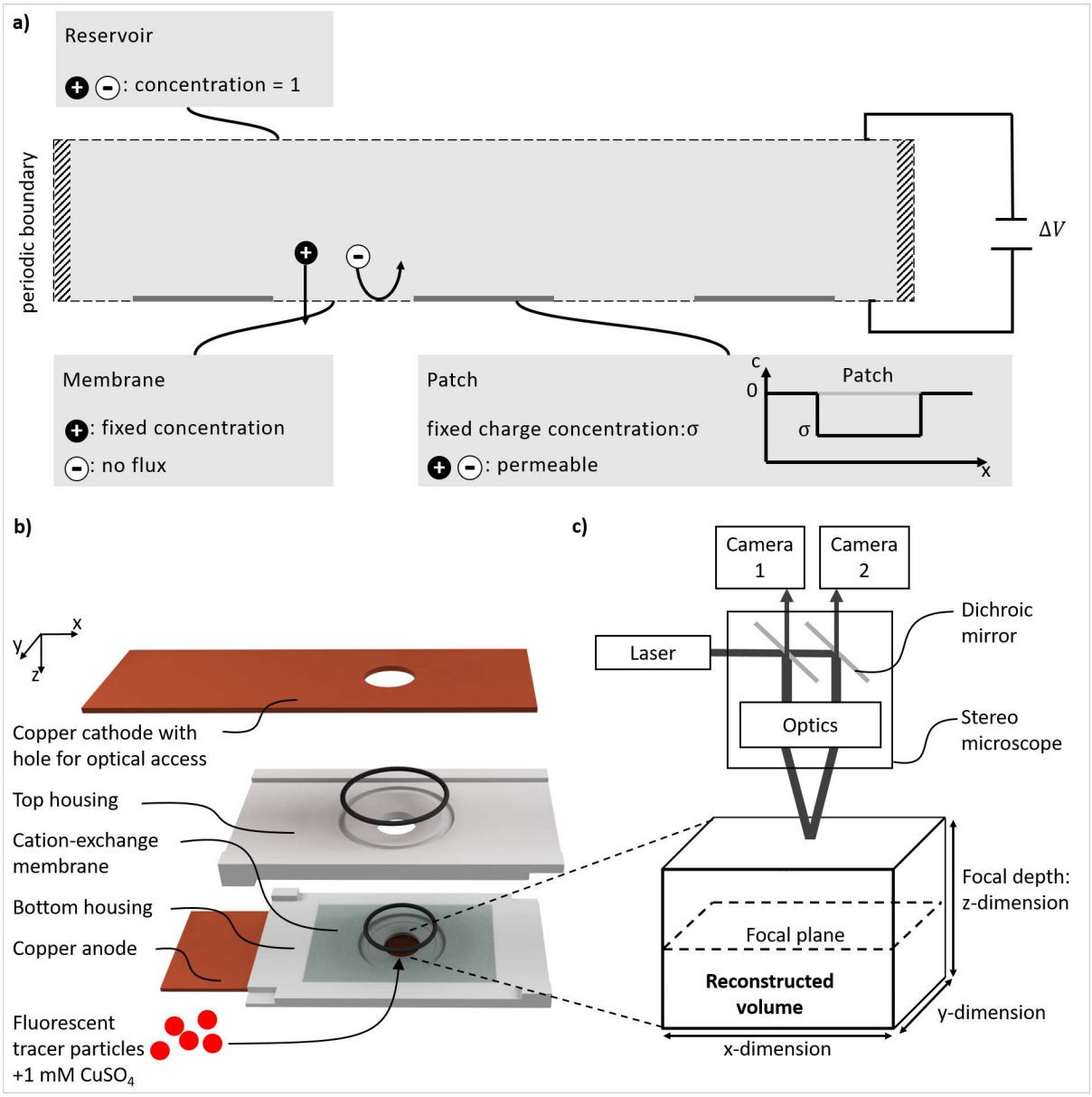

Figure 5: **Setup for the direct numerical simulations and the experiments. a)** Domain and boundary conditions of the direct numerical simulations. The domain is rectangular shaped between a mixed reservoir, an ideal cation-exchange membrane, and two periodic boundaries. **b)** Cell design for electrochemical experiments with simultaneous µPTV recording. The cathode is sealed by gluing a microscope glass slide, which is not shown in the rendering, on top. **c)** The setup for stereo micro particle image velocimetry consists of a laser that illuminates tracer particles in a sample volume through a stereomicroscope. The fluorescence response returns through the microscope and is recorded by two slightly angled high-speed cameras.

Governing equations

The model describes the conservation of momentum of an incompressible, single-phase Newtonian fluid through the Navier-Stokes and continuity equations.

$$\begin{aligned} 0 &= -\nabla p + \mu \nabla^2 \mathbf{u} - \rho \nabla \mathbf{\Phi} \\ 0 &= \nabla \cdot \mathbf{u} \end{aligned} \tag{1}$$

Here, p is the pressure, μis the dynamic viscosity $\mathbf{u}$ is the velocity vector, ρ is the electric charge density, and Φ is the electrostatic potential. The studies of Yariv et al. and Drusghalski et al. showed that the Navier-Stokes equation's inertia term could be neglected for this physics problem [27, 28].

The Nernst-Planck equation describes the ion transport under the action of an electric field within a low-ionic strength electrolyte.

$$\frac{\partial c_i}{\partial t} + \mathbf{u} \cdot \nabla c_i = \nabla \cdot (D_i \nabla c_i) - \nabla \cdot \left(D \frac{e z_i}{k_B T} c_i \nabla \mathbf{\Phi} \right) \tag{2}$$

where c_i is the concentration, $D = D^+ = D^- = 1 \times 10^{-9}\,\mathrm{m^2\,s^{-1}}$ is the diffusion coefficient. Additionally, e is the elementary charge, z_i is the charge valence, k_B is the Boltzmann constant and T is the absolute temperature. The index i is used to mark each individual species in the electrolyte.

The electric potential distribution in a given domain can be computed from Gauss' law, ignoring polarization.

$$\nabla \cdot (\varepsilon \nabla \mathbf{\Phi}) = -\rho_E \tag{3}$$

with permittivity ε. We use a modified version of the electric model and define the charge density as

$$\rho_E = F\left(\sum_{i=1}^{m} z_i c_i + \sigma\right) \tag{4}$$

where F represents Faraday's constant and m is the number of different ionic species. Additionally, σ is the background fixed charge introduced by the patches. In the rest of the domain, σ is set to zero.

Computational methods

The above equations are solved on a 2-dimensional mesh with 480 uniformly distributed cells in the x-direction, and 90 cells in the y-direction stretched with a scaling factor of 1.042. This setup achieves a minimum cell height of 0.001 H at the membrane and ensures a sufficient resolution. Furthermore, compared to the study of Druzgalski et al. [27], we increased the temporal resolution to time steps of $1 \cdot 10^{-7}$ s to ensure convergence when introducing patches.

The selected parameters (see Tab. 1 in the supporting information) correspond to dimensionless values typical for the direct numerical simulation of EC [7, 27, 29]. A complete list of all dimensionless values can be found in the supporting information Tab. 2. The applied potential was set to $\Phi = 20 \cdot V_t$ with the thermal voltage $V_t = \frac{k_B T}{ze}$ which is equivalent to a potential difference at which almost no velocity is induced at a homogeneous membrane. The electrohydrodynamic coupling constant $\kappa = \frac{\varepsilon}{\mu D} \cdot (\frac{k_B T}{ze})^2 = 0.5$ and Schmidt number $Sc = \frac{\mu}{\rho D} = 10^3$ are fixed by choice of solution and absolute temperature. The chosen values are typical for aqueous solutions at 300 K. The dimensionless Debye length $\lambda_d = \sqrt{\frac{\varepsilon k_B T}{2 c_b (z e L_z)^2}} = 10^{-3}$ is mostly dependent on the size of the examined system and electrolyte concentration. For example, a value of $\lambda_d = 10^{-3}$ corresponds to a reservoir to membrane distance of $\mathrm{H} = 1 \times 10^{-5}$ m using a 1 mM electrolyte. This value is commonly chosen in numerical examinations of EC, resulting

in a small system size with reasonable computational cost while providing physically relevant results [7, 27]. Experimental investigations have larger system sizes in the order of millimeters with electrolyte concentrations of 1 mM and above [11, 25, 30].

We plot our graphs with dimensionless values of time $t = \frac{t^*}{t_{diff}}$, velocity $u = \frac{u^*}{u_{diff}}$, concentration $c_i = \frac{c_i^*}{c_{bulk}}$, and distance $l = \frac{l^*}{H}$ using the characteristic scales $t_{diff} = \frac{H^2}{D} = 0.1\,\mathrm{s}$ and $u_{diff} = \frac{D}{H} = 1 \times 10^{-4}\,\mathrm{m\,s^{-1}}$.

Experimental details

We conduct experiments using an electrochemical cell that is suitable to evoke simultaneously and optically record electroconvective vortices [2]. We record and analyze the difference in vortex fields evolving at different modified cation-exchange membranes in this cell. The following sections describe the cell's design, the electrochemical experiments, the velocity recording, and the method of membrane modification.

Electrochemical cell

The electrochemical experiments are conducted in a cell (Fig. 5) **b)**, which allows optical access for the recording and reconstruction of the 3D velocity field inside the anode chamber using micro particle tracking velocimetry (µPTV). The cell consists of two housing parts with a bare or modified Nafion N117 (Chemours, Wilmington, Delaware, USA) cation-exchange membrane in between. If a modified membrane is used, the treated surface points towards the anode. The membrane modification procedure is described in the last methods section.

Two copper electrodes (25 mm×75 mm×0.5 mm) seal the top and the bottom of the chip. The cathode has a circular hole (d = 9 mm) which is sealed by a glass slide glued on top. The electrolyte (1 mM $CuSO_4$) is filled in the electrolyte chambers above and below the membrane. The bottom chamber's height matches the microscope's maximum focal depth of $L_z = 0.8\,\mathrm{mm}$.

The diameter of the chamber of 8 mm results in a large aspect ratio of 10, which is desired to prevent the confinement of the EC vortices [7, 31].

The electrochemical system of $CuSO_4$ in aqueous solution in combination with copper electrodes is often used in literature to evoke EC [30, 32, 33]. Copper ions dissolve at the anode, move through the membrane, and deposit on the cathode during the experiment.

The current density is described as the copper ion flux i per membrane area. The limiting current density in the plateau region can be calculated by [34]:

$$i_{\mathrm{lim}} = \frac{c_{\mathrm{B}}}{\delta} \cdot \frac{D \cdot F \cdot z}{t_{\mathrm{M}} - t_{\mathrm{E}}} \tag{5}$$

The bulk concentration c_B is approximated with a linear gradient between electrode and membrane as twice the electrolyte starting concentration c_0 in the anode chamber [34]. D is the diffusion coefficient, F is Faraday's constant, and z the ionic valence. The transport numbers in the membrane and electrolyte t_M and t_E describing the ion velocity difference are 0.96 and 0.4, respectively [34]. At current densities larger than $i_{lim} = 0.73\,\mathrm{A\,m^{-2}}$ for a 1 mM solution of $CuSO_4$, CP will result in the EC vortex formation close to the membrane in the anode chamber [30].

Velocity measurement

We use an optical technique called micro particle tracking velocimetry (µPTV) to reconstruct the 3D flow field of EC during operation. The measurement system consists of a high-frequency 532 nm Nd:YAG laser (DM150, Photonics Industries International Inc.), two high-speed cameras (Phantom VEO 710L, Vision Research Inc.), and a stereomicroscope (SteREO Discovery.V20, Carl Zeiss Microscopy Deutschland GmbH, Germany) with a 1× objective (PlanAprochromat 1×, Carl Zeiss Microscopy Deutschland GmbH, Germany), see Fig 5 **c)**.

The cameras record tracer particles' movement inside the microscope's focal depth from two different viewing angles allowing 3D reconstruction. The seeding density of the inert, fluorescent polystyrene microspheres (Thermo Scientific, Waltham, MA, USA) is 0.001 wt%. Those particles with a diameter of 3.2 µm and a zeta potential of −14.9 mV measured with a Malvern Zetasizer Nano ZS (Malvern Panalytical Ltd) are illuminated through the microscope by the laser. The recorded volume at a magnification of 5.12× and a halfway closed aperture is 4.9 mm×3.1 mm×0.8 mm with 1280 px×800 px resolution in x- and y-direction. The depth of the recorded volume of 0.8 mm matches the depth of our electrochemical cell's anode chamber. Therefore, it is possible to reconstruct the full velocity field of EC between membrane and anode.

The operation of the µPTV setup and the processing of the recorded images is done in the software DaVis (version: 10.0.5.47779, LaVision GmbH, Göttingen, Germany). After removing steady particle signals by subtracting the time-averaged intensity for each pixel, we use the Shake-the-Box algorithm to reconstruct the particle tracks [35, 36].

In post-processing, the implemented VIC# method is used for transforming the particle tracks to velocities (u_x, u_y, u_z) on a regular grid [37]. The velocities are reconstructed with a grid size of ten original voxels resulting in a final velocity field resolution of 128 px×80 px×21 px with a grid size of 38.4 µm.

DaVis plots coherent vortex structures using the λ_2-method [38]. To visualize the vortex structure of EC, coherent structures are then plotted as isosurfaces at a specific eigenvalue λ_2.

Experiments with velocity reconstruction

During each experiment, a set multiple of the limiting current density is forced through the electrodes by regulating the potential in chronopotentiometric experiments with a potentiostat

(Interface 1010E, Gamry, Pennsylvania, USA). The electrolyte is not pumped during the experiments, and the observed movement only results from EC vortices. When the electrochemical experiments start, we record the build-up of the EC vortex field at $4 \cdot i_{lim}$ for a maximum of 126 s at a frequency of 20 Hz.

After the experiments, we color the membrane inside the module with a diluted fluorescent dye (Staedler, Lumocolor, Germany) to visualize the otherwise transparent patches' positions.

Membrane surface modification

The modified Nafion membranes are produced by ink-jet printing of microgel suspensions using an Autodrop Compact 2.21 ink-jet printer with an MD-K-140 print head (microdrop Technologies, Germany) as described by Roghmans et al. [11].

Table 1: Microgel types used for membrane modification. In contrast to the microgels' zeta potential, Nafion has a reported zeta potential of -80 mV [39].

Microgel type	Synthesis	Zeta potential	Cross-linking degree	Reference
PNIPAM-co-Aac (11.5 wt% Aac)	surfactant free emulsion polymerization	-9.5 mV	1:25	Burmistrova et al. [40]
P2VP	surfactant free emulsion polymerization	+45.3 mV	1:100	Roghmans et al. [41]

The ink is prepared by diluting suspensions of either PNIPAM-co-Aac or P2VP microgels, see Tab. 1 to a concentration of 0.05 wt% with HPLC grade water. We produce patterns of circular patches with either 400 µm or 600 µm diameter and a spacing of 450 µm or 900 µm, respectively.

Nafion membranes have a reported zeta potential of -80 mV [39]. The used microgels are expected to change the surface charge towards positive zeta potentials with -9.5 mV for PNIPAM-co-Aac and +45.3 mV for P2VP measured with a Malvern Zetasizer Nano ZS (Malvern Panalytical Ltd).

Acknowledgements

This work received funding from the European Research Council (ERC) under the European Union's Horizon 2020 research and innovation program (grant agreement no. 694946). The DFG also supported this work through the project SFB 985 Functional Microgels and Microgel Systems in project B6 (project no. project no. 191948804). The measurements were conducted with a high-speed stereomicroscope PIV funded by the Major Research Instrumentation Program according to Art. 91b GG in the Research Building NW1481006 "NGP2 – Center for Next Generation Processes and Products" (project no. 319121241). Simulations were performed with computing resources granted by RWTH Aachen University under projects thes0630, thes0631, and thes0698. M. Wessling acknowledges DFG funding through the Gottfried Wilhelm Leibniz Award 2019 (WE 4678/12-1). M. Wessling also appreciates the support from the Alexander-von-Humboldt foundation.

The authors acknowledge A. Lüken for providing the pNIPAM-co-Aac microgels, D. Bell for providing the P2VP microgels, K. Faensen for SEM and EDX imaging, and K. Baitalow, A. Kalde, D. Wyppysek, G. Linz, F. Roghmanns and J. Lohaus for their input and the fruitful discussions.

Author Contributions

Felix Stockmeier: Conceptualization, Methodology, Formal analysis, Investigation, Data Curation, Writing - Original Draft, Visualization, Project administration. **Daniel Felder:** Conceptualization, Methodology. **Steffen Eser:** Software, Formal analysis, Investigation, Visualization. **Malte Habermann, Petar Perić, Stephan Musholt, Katharina Albert:** Formal analysis, Investigation, Visualization. **John Linkhorst:** Writing - Review & Editing, Project administration, Supervision. **Matthias Wessling:** Conceptualization, Resources,

Project administration, Supervision, Writing - Review & Editing, Funding acquisition.

Competing Interests statement

The authors declare that there are no competing interests.

References

[1] Ali Mani and Karen May Wang. Electroconvection near electrochemical interfaces: Experiments, modeling, and computation. *Annual Review of Fluid Mechanics*, 52(1):509–529, 2020. doi: 10.1146/annurev-fluid-010719-060358.

[2] Felix Stockmeier, Michael Schatz, Malte Habermann, John Linkhorst, Ali Mani, and Matthias Wessling. Direct 3d observation and unraveling of electroconvection phenomena during concentration polarization at ion-exchange membranes. *Journal of Membrane Science*, 2021. doi: 10.1016/j.memsci.2021.119846.

[3] Elena Belova, Galina Lopatkova, Natalia Pismenskaya, Victor Nikonenko, and Christian Larchet. Role of water splitting in development of electroconvection in ion-exchange membrane systems. *Desalination*, 199(1-3):59–61, 2006. doi: 10.1016/j.desal.2006.03.142.

[4] Sang Van Pham, Zirui Li, Kian Meng Lim, Jacob K. White, and Jongyoon Han. Direct numerical simulation of electroconvective instability and hysteretic current-voltage response of a permselective membrane. *Physical review. E, Statistical, nonlinear, and soft matter physics*, 86(4 Pt 2):046310, 2012. doi: 10.1103/PhysRevE.86.046310.

[5] M. Wessling, L. Garrigós Morcillo, and S. Abdu. Nanometer-thick lateral polyelectrolyte micropatterns induce macrosopic electro-osmotic chaotic fluid instabilities. *Scientific reports*, 4:4294, 2014. doi: 10.1038/srep04294.

[6] Said Abdu, Manuel-César Martí-Calatayud, John Erik Wong, Montserrat García-Gabaldón, and Matthias Wessling. Layer-by-layer modification of cation exchange membranes controls ion selectivity and water splitting. *ACS applied materials & interfaces*, 6 (3):1843–1854, 2014. doi: 10.1021/am4048317.

[7] Scott M. Davidson, Matthias Wessling, and Ali Mani. On the dynamical regimes of pattern-accelerated electroconvection. *Scientific reports*, 6:22505, 2016. ISSN 2045-2322. doi: 10.1038/srep22505.

[8] Joeri C. de Valenca, Morten Jõgi, R. Martijn Wagterveld, Elif Karatay, Jeffery A. Wood, and Rob G. H. Lammertink. Confined electroconvective vortices at structured ion exchange membranes. *Langmuir : the ACS journal of surfaces and colloids*, 34(7):2455–2463, 2018. doi: 10.1021/acs.langmuir.7b04135.

[9] Anne M. Benneker. *From small to big: Ion transport at interfaces*. University of Twente, 2018. ISBN 9789036544924. doi: 10.3990/1.9789036544924.

[10] V. V. Gil, M. A. Andreeva, L. Jansezian, J. Han, N. D. Pismenskaya, V. V. Nikonenko, C. Larchet, and L. Dammak. Impact of heterogeneous cation-exchange membrane surface modification on chronopotentiometric and current–voltage characteristics in nacl, cacl2 and mgcl2 solutions. *Electrochimica Acta*, 281(8):472–485, 2018. doi: 10.1016/j.electacta.2018.05.195.

[11] Florian Roghmans, Elizaveta Evdochenko, Felix Stockmeier, Sven Schneider, Amel Smailji, Rahul Tiwari, Annabel Mikosch, Elif Karatay, Alexander Kühne, Andreas Walther, Ali Mani, and Matthias Wessling. 2d patterned ion–exchange membranes induce electroconvection. *Advanced Materials Interfaces*, 6(1):1801309, 2019. doi: 10.1002/admi.201801309.

[12] Joonhyeon Kim, Sangha Kim, and Rhokyun Kwak. Controlling ion transport with pattern

structures on ion exchange membranes in electrodialysis. *Desalination*, 499:114801, 2021. doi: 10.1016/j.desal.2020.114801.

[13] Yifei Guan, Tianhang Yang, and Jian Wu. Mixing and transport enhancement in microchannels by electrokinetic flows with charged surface heterogeneity. *Physics of Fluids*, 33(4):042006, 2021. doi: 10.1063/5.0047181.

[14] Victor I. Zabolotsky and Victor Nikonenko. Effect of structural membrane inhomogeneity on transport properties. *Journal of Membrane Science*, 79(2-3):181–198, 1993. doi: 10.1016/0376-7388(93)85115-D.

[15] N. A. Mishchuk. Electro-osmosis of the second kind near the heterogeneous ion-exchange membrane. *Colloids and Surfaces A: Physicochemical and Engineering Aspects*, 140(1-3): 75–89, 1998. doi: 10.1016/S0927-7757(98)00216-7.

[16] Jae-Hwan Choi, Sung-Hye Kim, and Seung-Hyeon Moon. Heterogeneity of ion-exchange membranes: The effects of membrane heterogeneity on transport properties. *Journal of Colloid and Interface Science*, 241(1):120–126, 2001. doi: 10.1006/jcis.2001.7710.

[17] E. Volodina, N. Pismenskaya, V. Nikonenko, C. Larchet, and G. Pourcelly. Ion transfer across ion-exchange membranes with homogeneous and heterogeneous surfaces. *Journal of Colloid and Interface Science*, 285(1):247–258, 2005. doi: 10.1016/j.jcis.2004.11.017.

[18] J. Balster, M. H. Yildirim, D. F. Stamatialis, R. Ibanez, R. G. H. Lammertink, V. Jordan, and M. Wessling. Morphology and microtopology of cation-exchange polymers and the origin of the overlimiting current. *The journal of physical chemistry. B*, 111(9):2152–2165, 2007. doi: 10.1021/jp068474t.

[19] V. I. Zabolotsky, L. Novak, A. V. Kovalenko, V. V. Nikonenko, M. H. Urtenov, K. A.

Lebedev, and A. Yu. But. Electroconvection in systems with heterogeneous ion-exchange membranes. *Petroleum Chemistry*, 57(9):779–789, 2017. doi: 10.1134/S0965544117090109.

[20] K. A. Nebavskaya, V. V. Sarapulova, K. G. Sabbatovskiy, V. D. Sobolev, N. D. Pismenskaya, P. Sistat, M. Cretin, and Victor Nikonenko. Impact of ion exchange membrane surface charge and hydrophobicity on electroconvection at underlimiting and overlimiting currents. *Journal of Membrane Science*, 523:36–44, 2017. doi: 10.1016/j.memsci.2016.09.038.

[21] S. A. Mareev, D.Yu. Butylskii, N. D. Pismenskaya, C. Larchet, L. Dammak, and Victor Nikonenko. Geometric heterogeneity of homogeneous ion-exchange neosepta membranes. *Journal of Membrane Science*, 563:768–776, 2018. doi: 10.1016/j.memsci.2018.06.018.

[22] N. D. Pismenskaya, S. A. Mareev, E. V. Pokhidnya, C. Larchet, L. Dammak, and V. V. Nikonenko. Effect of surface modification of heterogeneous anion-exchange membranes on the intensity of electroconvection at their surfaces. *Russian Journal of Electrochemistry*, 55(12):1203–1220, 2019. doi: 10.1134/S1023193519120139.

[23] Tomáš Belloň and Zdeněk Slouka. Overlimiting convection at a heterogeneous cation-exchange membrane studied by particle image velocimetry. *Journal of Membrane Science*, 643(3):120048, 2022. doi: 10.1016/j.memsci.2021.120048.

[24] E. A. Demekhin, N. V. Nikitin, and V. S. Shelistov. Three-dimensional coherent structures of electrokinetic instability. *Physical review. E, Statistical, nonlinear, and soft matter physics*, 90(1):013031, 2014. doi: 10.1103/PhysRevE.90.013031.

[25] Soohyeon Kang and Rhokyun Kwak. Pattern formation of three-dimensional electroconvection on a charge selective surface. *Physical Review Letters*, 124(15):52, 2020. doi: 10.1103/PhysRevLett.124.154502.

[26] Francisco Pimenta and Manuel A. Alves. Numerical simulation of electrically-driven flows using openfoam. *arXiv: 1802.02843v2*, 2018.

[27] C. L. Druzgalski, M. B. Andersen, and A. Mani. Direct numerical simulation of electroconvective instability and hydrodynamic chaos near an ion-selective surface. *Physics of Fluids*, 25(11):110804, 2013. doi: 10.1063/1.4818995.

[28] Ehud Yariv. Asymptotic current-voltage relations for currents exceeding the diffusion limit. *Physical review. E, Statistical, nonlinear, and soft matter physics*, 80(5 Pt 1):051201, 2009. doi: 10.1103/PhysRevE.80.051201.

[29] Elif Karatay, Clara L. Druzgalski, and Ali Mani. Simulation of chaotic electrokinetic transport: performance of commercial software versus custom-built direct numerical simulation codes. *Journal of Colloid and Interface Science*, 446:67–76, 2015. doi: 10.1016/j.jcis.2014.12.081.

[30] Joeri C. de Valenca, R. Martijn Wagterveld, Rob G. H. Lammertink, and Peichun A. Tsai. Dynamics of microvortices induced by ion concentration polarization. *Physical review. E, Statistical, nonlinear, and soft matter physics*, 92(3):031003, 2015. doi: 10.1103/PhysRevE.92.031003.

[31] Peichun Tsai, Zahir A. Daya, and Stephen W. Morris. Aspect-ratio dependence of charge transport in turbulent electroconvection. *Physical review letters*, 92(8):084503, 2004. doi: 10.1103/PhysRevLett.92.084503.

[32] Daosheng Deng, E. Victoria Dydek, Ji-Hyung Han, Sven Schlumpberger, Ali Mani, Boris Zaltzman, and Martin Z. Bazant. Overlimiting current and shock electrodialysis in porous media. *Langmuir : the ACS journal of surfaces and colloids*, 29(52):16167–16177, 2013. doi: 10.1021/la4040547.

[33] Zhibo Gu, Bingrui Xu, Peng Huo, Shmuel M. Rubinstein, Martin Z. Bazant, and Daosheng Deng. Deionization shock driven by electroconvection in a circular channel. *Physical Review Fluids*, 4(11), 2019. doi: 10.1103/PhysRevFluids.4.113701.

[34] Joeri C. de Valenca. *Overlimiting current properties at ion exchange membranes*. University of Twente, 2017. ISBN 9789036543149. doi: 10.3990/1.9789036543149.

[35] D. Schanz, A. Schröder, S. Gesemann, D. Michaelis, and B. Wieneke. 'shake the box': A highly efficient and accurate tomographic particle tracking velocimetry (tomo-ptv) method using prediction of particle positions. *PIV13; 10th International Symposium on Particle Image Velocimetry*, 2013. URL `https://repository.tudelft.nl/islandora/object/uuid:b5eb6d27-bfb1-4c25-bc79-637df9c76694?collection=research, accessed: 19.10.2020`.

[36] A. Schröder, D. Schanz, D. Michaelis, C. Cierpka, S. Scharnowski, and C. J. Kähler. Advances of piv and 4d-ptv "shake-the-box" for turbulent flow analysis –the flow over periodic hills. *Flow, Turbulence and Combustion*, 95(2-3):193–209, 2015. doi: 10.1007/s10494-015-9616-2.

[37] Y. J. Jeon, J.F.G. Schneiders, M. Müller, D. Michaelis, and B. Wieneke. *4D flow field reconstruction from particle tracks by VIC+ with additional constraints and multigrid approximation*. ETH Zurich, 2018. doi: 10.3929/ETHZ-B-000279199.

[38] Jinhee Jeong and Fazle Hussain. On the identification of a vortex. *Journal of Fluid Mechanics*, 285(-1):69, 1995. doi: 10.1017/S0022112095000462.

[39] Alexander C. Barbati and Brian J. Kirby. Electrokinetic measurements of thin nafion films. *Langmuir : the ACS journal of surfaces and colloids*, 30(8):1985–1993, 2014. doi: 10.1021/la403735g.

[40] Anna Burmistrova, Marcel Richter, Michael Eisele, Cagri Üzüm, and Regine von Klitzing. The effect of co-monomer content on the swelling/shrinking and mechanical behaviour of individually adsorbed pnipam microgel particles. *Polymers*, 3(4):1575–1590, 2011. doi: 10.3390/polym3041575.

[41] F. Roghmans, M. C. Martí-Calatayud, S. Abdu, R. Femmer, R. Tiwari, A. Walther, and M. Wessling. Electrochemical impedance spectroscopy fingerprints the ion selectivity of microgel functionalized ion-exchange membranes. *Electrochemistry Communications*, 72: 113–117, 2016. doi: 10.1016/j.elecom.2016.09.009.

Supplementary Files

This is a list of supplementary files associated with this preprint. Click to download.

- 2021SIStockmeierLocalizedElectroconvectionatIonExchangeMembraneswithHeterogeneousSurfaceCharge.pdf
- Sup1P2VPscaling.png
- Sup2DNSioverPC.png